

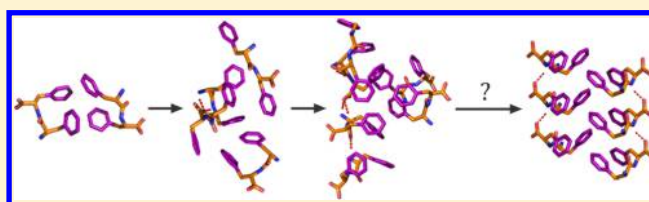
# Molecular Insights into Diphenylalanine Nanotube Assembly: All-Atom Simulations of Oligomerization

Joohyun Jeon, Carolyn E. Mills, and M. Scott Shell\*

Department of Chemical Engineering, University of California Santa Barbara, Santa Barbara, California 93106-5080, United States

**S** Supporting Information

**ABSTRACT:** Self-assembling peptides represent a growing class of inexpensive, environmentally benign, nanostructured materials. In particular, diphenylalanine (FF) self-assembles into nanotubes with remarkable strength and thermal stability that have found use in a wide variety of applications, including as sacrificial templates and scaffolds for structuring inorganic materials and as interfacial “nanoforests” for superhydrophobic surfaces and high-performance supercapacitors and biosensors. However, little is known about the assembly mechanisms of FF nanotubes or the forces underlying their stability. Here, we perform a variety of molecular dynamics simulations on both zwitterionic and capped (uncharged) versions of the FF peptide to understand the early stages of self-assembly. We compare these results to simulations of the proposed nanotube X-ray crystal structure. When comparing the zwitterionic and uncharged FF peptides, we find that, while electrostatic interactions steer the former into more ordered dimers and trimers, the hydrophobic side chain interactions play a strong role in determining the structures of larger oligomers. Simulations of the crystal structure fragment also suggest that the strongest interactions occur between side chains, not between the charged termini that form salt bridges. We conclude that the amphiphilic nature of FF is key to understanding its self-assembly, and that the early precursors to nanotube structures are likely to involve substantial hydrophobic clustering, rather than hexamer ring motifs as has been previously suggested.



## ■ INTRODUCTION

Very short peptides that self-assemble into well-defined nanostructures have recently emerged as potentially powerful tools for the development of new, environmentally benign, functional materials. In particular, a new class of systems has stemmed from the discovery of the simple diphenylalanine (FF) peptide a decade ago by Reches and Gazit.<sup>1</sup> The FF peptide self-assembles into hollow nanotubes (FFNTs) with 100–150 nm outer diameters and  $\mu\text{m}$  scale lengths that are extremely stable and have a growing list of rather remarkable properties. They survive heating in solution to above 100 °C,<sup>2</sup> dry heating on mica to 150 °C, and exposure to solvents like alcohols and acetone.<sup>3</sup> Impressively, they have a stiffness of 160 N/m and a Young's modulus of 19 GPa,<sup>4</sup> placing them among the strongest biomaterials presently known.<sup>5,6</sup> More recently, FFNTs were shown to exhibit many properties normally only associated with semiconductors, quantum dots, and inorganic crystals, such as quantum confinement,<sup>7,8</sup> photoluminescence,<sup>8</sup> strong piezoelectric activity,<sup>9,10</sup> and photosensitizing effects.<sup>11</sup>

There has been growing excitement for potential applications of FFNTs for a range of technologies. In principle, they offer low-cost material scaffolds that are nontoxic and can be controlled or modified through biochemical strategies leveraging affinity binding, enzymatic sensing, and reporting functionalities. FFNTs have been used as sacrificial templates (through enzymatic degradation) for metal nanowires<sup>1</sup> and photoswitching nanoribbons,<sup>12</sup> as new hydrogels<sup>13</sup> and biosensors,<sup>14,15</sup> and as scaffolds for electronic interconnects<sup>16</sup>

and microfluidic channels.<sup>17</sup> For most of these efforts, FFNTs are fabricated at room temperature by initial dissolution in alcohol followed by dilution with pure water. Recently, however, a vapor deposition method<sup>18</sup> has been developed to fabricate large arrays of vertically aligned FFNT forests with the controllable length and density, leading to new applications where high surface area interfaces are useful. For example, FFNT forests were shown to remarkably improve the capacitance of supercapacitors by increasing electrode surface area,<sup>19</sup> and they were also used to pattern superhydrophobic interfaces to form fluid channels or self-cleaning surfaces.<sup>18</sup>

The atomic structure of FFNTs provides essential information for understanding their role in these applications, and it was first studied by Görbitz using X-ray diffraction.<sup>20,21</sup> While earlier experiments readily established that the outer diameter of an FFNT is typically on the order of 100 nm, Görbitz's results suggest that the tube wall is porous along the axial direction, with many small 10 Å diameter, hydrophilic channels in a hexagonal arrangement that run parallel to the much larger interior of the tube. The fundamental structural building block of these channels appears to be a hexagonal ring of six diphenylalanine (FF) peptides that are associated head-to-tail at their charged termini. These rings repeat laterally to form the small pores, with the aromatic side chains of the FF

**Received:** August 20, 2012

**Revised:** March 22, 2013

**Published:** March 22, 2013

peptides pointing outward and the hydrophilic backbone forming the interior interface; the side chains then interact favorably through hydrophobic and  $\pi$ -stacking interactions with side chains of peptides from neighboring channels. Because these small pores are hydrophilic in nature, both water molecules and ions can flow through them.<sup>19</sup>

Despite the growing applications of FFNTs and these initial efforts toward structural characterization, very little is actually known about the mechanism of FFNT self-assembly or the molecular forces that impart such dramatic stability. Experiments have attempted in part to address the latter issue through directed mutation. Reches and Gazit made eight variants of the FF peptide,<sup>22</sup> and found that analogues with noncharged termini (e.g., capped) similarly form highly ordered tubular structures, suggesting that strong ion-pairing interactions are not a necessary driving force. On the other hand, mutated peptides in which the phenyl side-chain is replaced with a non-aromatic cyclohexane analogue do not form nanotubes,<sup>23</sup> suggesting an important role for aromaticity,  $\pi$ -stacking, or hydrophobic interactions. Interestingly, such mutational studies have also shown, often unexpectedly, that various diphenylalanine analogues can form many different but still ordered nanostructures, such as spherical nanovesicles,<sup>24</sup> nanofibrils,<sup>13</sup> nanoplates,<sup>25</sup> or even dendrites.<sup>26</sup> With regard to the assembly mechanism, Yan et al.<sup>5</sup> hypothesized that FF monomers first form a 2D layer that subsequently closes to form a tube geometry, but further studies are needed to corroborate this idea.

Simulations offer a natural means to understand many aspects of FF self-assembly; however, only a few studies appear to have been performed so far. Initial efforts using energy minimization<sup>27</sup> and molecular dynamics<sup>28</sup> of all-atom models showed the formation of cylindrical structures reminiscent of tubes, though the diameters and packing structure of these studies disagreed with experiments.<sup>20</sup> Song et al.<sup>29</sup> developed a highly simplified lattice model and used Monte Carlo (MC) simulations to show the formation of tubular structures. More recently, Tamamis et al.<sup>30</sup> examined the association of 12 atomically detailed FF peptides using an implicit water model, and observed the transient formation of ring-like structures of four, five, and six FF peptides that are reminiscent of the basic building blocks of the nanotube structure; however, the frequencies with which these networked configurations appeared were actually quite low. Still, they suggested through an energetic analysis that hydrophobic interactions are essential to the association behavior and that the ring formation by six FF peptides may occur in the early stage of FF self-assembly. Guo et al.<sup>31</sup> recently used large-scale MC simulations of a coarse-grained FF model to show the emergence of different nanostructures and their concentration dependence. They suggested that FF peptide behaves like a surfactant, first forming vesicles, and then by fusion, nanotube-like structures.

In this study, we aim to understand the detailed balance of hydrogen bonds, electrostatic interactions, and side chain aromatic or hydrophobic forces in the very first stages of FF peptide assembly. We examine two kinds of FF peptides: a charged version with zwitterionic termini and another with uncharged (capped) ends. We use various molecular dynamics simulations to capture the association behavior of small FF oligomer systems, and compare these to a reference simulation of a fragment of the X-ray structure. Our analysis is focused on the following two questions: (1) What is the role of electrostatic and polar interactions in FF self-assembly? (2)

What are the structures of the very first aggregates (oligomers) of FF peptides?

## METHODS

We study the self-assembly of FF peptides at several different levels. Dimerization and 12-mer association processes are examined using all-atom molecular dynamics (MD) in explicit water. For the 12-mer simulations, we examine both a “low” and “high” concentration case. To use as a reference for comparison with the assembly simulations, we also perform all-atom molecular dynamics of a fragment of the crystal structure of the FFNT nanotube. Throughout we use the AMBER program.<sup>32,33</sup> All simulations in this work and associated concentrations are summarized in Table 1.

**Table 1. List of Simulations Performed in This Work**

name <sup>a</sup>	no. of FF peptides	concentration (mg/mL)
uFF2	2	19
cFF2	2	21
uFF12L	12	55
uFF12H	12	136
cFF12L	12	61
cFF12H	12	151
uFFX	168	

<sup>a</sup>Names beginning with “u” involve uncapped/zwitterionic peptides, and those with “c” the capped/uncharged versions. FF2 and FF12 indicate simulations of 2 and 12 peptides, respectively. In some cases, “L” or “H” is used to indicate simulations at low and high concentrations. “X” indicates the simulation of the crystal structure.

We have also performed comparative simulations using an implicit water model, the generalized Born solvent accessible surface area (GBSA) method of Onufriev et al.<sup>34</sup> These studies are detailed in the Supporting Information. However, we found that the GBSA implicit solvent model appears to perform poorly for the FF peptide systems, likely because of their small molecular size. For example, such an implicit model leads to an overall repulsive interaction between two FF peptides, which is in stark contrast to the predictions of explicit models (see the Supporting Information). Indeed, several analyses have suggested potentially large errors in the predictions of surface-area-based models.<sup>35–38</sup> Therefore, here, we focus on simulations using an explicit water model.

In our explicit-water MD simulations, we use the ff99SB force field.<sup>39</sup> The periodic box is solvated using a TIP3P water box with a minimum distance of 12 Å to the border for all but the high-concentration 12mer run, which uses a minimum distance of 6 Å to the border. The fragment of the crystal structure consists of 168 diphenylalanine peptides, and is constructed from the NMR data provided at the Cambridge Crystallographic Data Centre, no. CCDC 163340.<sup>40</sup> We use AmberTools 11 to construct a unit cell. Prior to each run, we perform minimization on all systems using a steepest descent protocol for 7000 cycles and followed by the conjugate gradient method for 3000 cycles. The systems are then heated from 0 to 300 K over 20 ps using the Langevin thermostat with a collision frequency of 2 ps<sup>−1</sup> (at constant volume). Each system is then allowed to equilibrate for 1 ns at 300 K but under constant pressure conditions at 1 bar, with a Berendsen barostat. Production runs for the systems then proceed under these same conditions. Dimer systems and 12mer systems are simulated for 100 ns, and the last 95 ns is used to cluster peptide

conformations. FF peptides in our simulations associate and dissociate repeatedly during the 100 ns, forming a variety of encounter complexes, without evidence of significant kinetic traps on this time scale (Figure S4, Supporting Information). During the analysis of these runs, we use a *k*-means clustering algorithm to determine structures and their populations from our simulations.<sup>41,42</sup> The crystal structure of FFNT is first simulated for 5 ns with water layers on the top and bottom so as to estimate the number of equilibrium water molecules present inside the nanotube pores when exposed to a large water bath ( $d = 30$  Å). After 5 ns, an additional 5 ns simulation is performed without the water layers using periodic boundary conditions so as to mimic the continuous FF nanostructure.

## RESULTS

Here we examine the results from a variety of simulations that probe small FF oligomer formation and hence the earliest structures underlying the FF self-assembly pathway. In what follows, abbreviations for each simulation are given in brackets and full details can be found in Table 1. The first step of this study involves understanding the simplest oligomers, the interaction between two FF molecules to form a dimer [uFF2]. The next step investigates the cooperative interactions of FF peptides and the comparative structures of small FF oligomers. We use MD simulations of 12 FF peptides and examine two concentration regimes with explicit solvent [uFF12L and uFF12H]. To specifically understand the contributions of electrostatic effects, we perform identical simulations with uncharged (capped) FF peptides [cFF2, cFF12L, and cFF12H].

All simulations are compared with a large-scale MD simulation of the FF crystal structure [uFFX] (Figure 1). In anticipation of results from the oligomer simulations, we first describe the findings from this “reference” simulation. In the crystal structure simulation, we observe several potentially stabilizing polar interactions. A salt bridge occurs between the

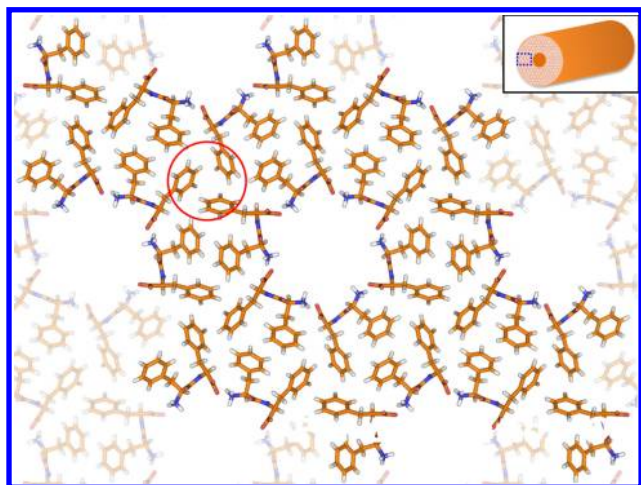


**Figure 1.** Cross section of the crystal structure of FF nanotubes simulated in this work. One unit cell is composed of full-color peptides; image copies are lightened. Water molecules are omitted for clarity but are present inside the hexagonal rings/pores defined by the backbones of six peptides. The red circle indicates one example where close packing of the hydrophobic side chains occurs at the junction between three ring groups. Interestingly, this region involves interactions between the second side chains of each two-residue peptide.

termini of adjacent peptides ( $-\text{NH}_3^+ \cdots ^-\text{OOC}-$ ) that are embedded in a slice of the nanotube (one layer of peptides) perpendicular to the tube axis. Two hydrogens in the N termini seem to be directly involved in this interaction, while the third points into the small porous channel and is accepted by water molecules. Water molecules also provide additional donors for the carboxylate groups in the C termini. Another polar interaction involves the amide N and carboxylate hydrogen bond motif,  $-\text{NH} \cdots ^-\text{OOC}-$ . These contacts facilitate interactions between different peptide layers in the crystal structure, i.e., the stacking of hexamer rings into elongated parallel, twisting, six-sided sheets that form the small nanotube pores (not shown in Figure 1).

To quantify the interactions between different atoms, we calculate contact probabilities from the MD simulation using a cutoff length of 6 Å (Figure 3g). Atom numbers for heavy atoms are defined in these as in Figure 2. The contact maps

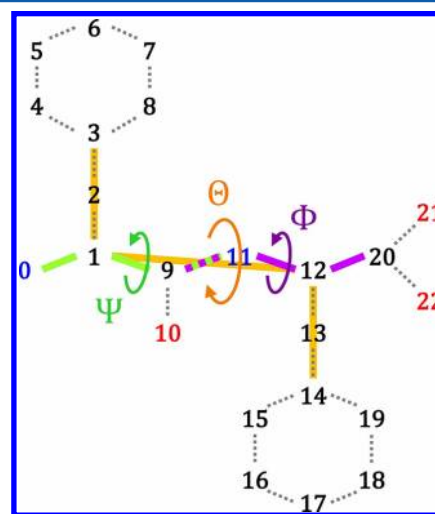


**Figure 2.** Definitions of the atom numbers and dihedral angles of the FF peptide used in this work. Oxygen atoms are indicated by red, nitrogen atoms by blue, and carbon atoms by black.

show the *relative* probabilities of different contacts between atoms; they reflect the number of contacts for each atom–atom pair divided by the total number of contacts. These maps therefore do not reflect the absolute frequency with which different contacts are made but rather merely how more or less preferred different contact pairs are. We divide the interactions in the maps into four main groups that become clear from them: a ring–ring interaction among side chain atoms (atom numbers 3–8 and 14–19), a salt-bridge interaction between oppositely charged termini (atoms 0, 21, and 22), a backbone–backbone hydrogen-bonding interaction (atoms 9–11), and an interaction between the central backbone and C-terminus (atoms 11, 21, and 22). Figure 3g shows that, in the crystal, side-chain contacts are dominant compared to other polar interactions (e.g., hydrogen bonds and salt bridges). In particular, we find that the interaction between the second side chains in two peptides contains the most frequent contacts. This is likely the result of the tight packing of second side chains that occurs in the interstitial hydrophobic region between three channel pores (highlighted in the red circle in Figure 1). In contrast, the first side chains interact in the region between two pores, and are apparently slightly less constrained in conformation, though still have well-pronounced contacts.



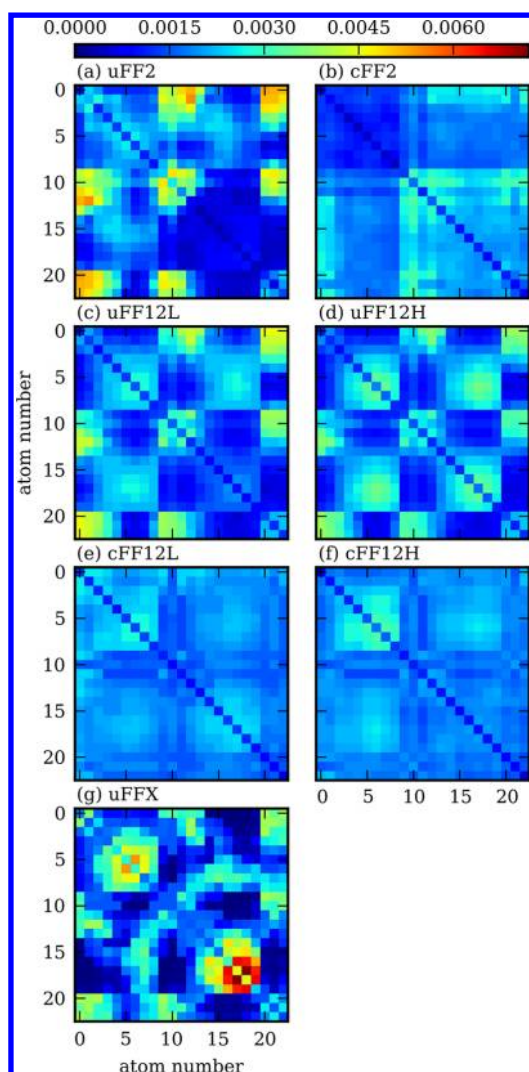


**Figure 3.** Atom–atom contact maps of FF peptides in nine different simulations. Atom numbers are defined in Figure 2. The maps are colored according to contact probability, with blue indicating smaller and red indicating larger values. Two atoms are defined as “in contact” if the distance between them is smaller than 6 Å. The bottom left panel gives the results for the simulation of the crystal structure to which the other panels can be compared.

Interestingly, Figure 3g shows that the salt-bridge interactions between the termini are much less frequent (by a factor of 2). This is the likely result of increased fluctuations of the corresponding atom positions in the crystal structure, which are in contact with the fluid water in the pore. The result is also suggestive that the salt bridges are less significant for stability of the nanotube structures than the side-chain interactions, which is consistent with experiments that have shown the formation of nanotubes with capped termini.

We now turn to the results of the MD simulations with two FF peptides in a large periodic box. Figure 4 shows through (unnormalized) PMFs that charged FF peptides have a weak but favorable attractive interaction. Clustering (Figure 5) reveals that dimers tend to form an antiparallel motif with the side chains of one peptide in the cis conformation and the side chains of the other in the trans state. In isolation, each peptide prefers the trans arrangement, and upon dimerization, one peptide appears to adopt the sterically less favorable cis conformation in an attempt to form hydrogen bonds and an

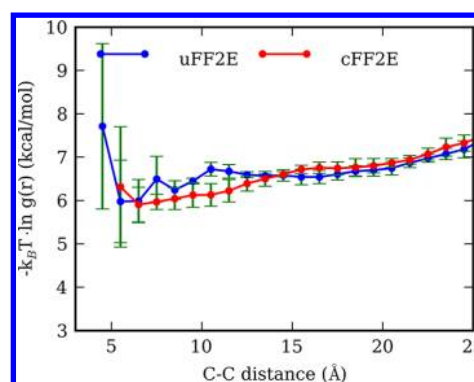


**Figure 4.** Potential of mean force calculations from MD simulations of dimerization.  $g(r)$  is the pair correlation function between the central backbone carbons (atom 9 in Figure 2) from each peptide. Here, it is simply normalized such that  $\int 4\pi r^2 g(r) dr = 1$ , and the ideal (i.e., noninteracting) part of the free energy,  $-k_B T \ln 4\pi r^2$ , is subtracted from the curves shown.

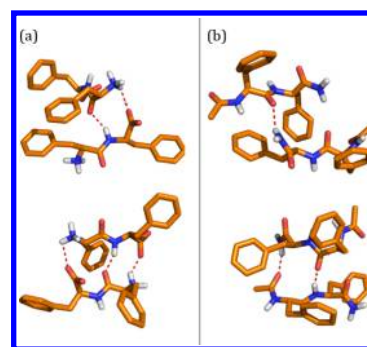


**Figure 5.** Top two clustered structures (top and bottom) from MD simulations of two (a) charged and (b) uncharged FF peptides.

intermolecular salt bridge. The contact map of the zwitterionic system (Figure 3a) offers further interpretation. The most significant interactions seem to be hydrogen bonds formed between either two peptide backbones or between the N terminus of one peptide and the backbone carbonyl oxygen of the other. Interestingly, this promotes strong first ring interactions between the two peptides, which contrasts the more prevalent second ring interactions seen in the crystal structure contact map.

A different behavior is observed for the uncharged (capped) version of the FF peptide. Figure 4 shows that it has a broad PMF minimum that is shifted outward to a distance near 6 Å. Cluster structures (Figure 5b) reveal that the stable dimer involves a larger separation distance because the backbone oxygen of one peptide tends to form a stable interaction with the N-cap of the other. The contact map for this case (Figure 3b) shows a significant reduction in preferences for particular atom–atom interactions as compared to the zwitterionic peptide (Figure 3a). Overall, both dimer simulations suggest that the dominant structures are driven by intermolecular and intramolecular hydrogen bonding.

To examine higher-order oligomers and cooperative effects, we subsequently investigate the results of MD simulations with 12 FF peptides. We consider two concentrations corresponding to “small” and “large” simulation boxes, although both concentrations are high relative to experiment in order to facilitate assembly (in experiments, diphenylalanine peptides are first dissolved in hexafluoro-2-propanol at a high

concentration of 100 mg/mL and then diluted to 2 mg/mL in ddH<sub>2</sub>O<sup>22</sup>). Our first analysis involves clustering peptides in contact into oligomers of different sizes, using a distance-based criterion. We define a cluster as a set of  $N$  peptides that has  $N - 1$  connections: two peptides are connected if the distance between the centers of mass of the side-chain rings is less than 7.5 Å. We observe species ranging from monomers to nonamers, and the relative frequencies of each are summarized in Table 2. The frequencies reflect the oligomer with the highest number of peptides in each simulation frame.

**Table 2. The Frequency of Observed Oligomers of Different Sizes in MD Simulations of 12 FF Peptides**

%	uFF12L	uFF12H	cFF12L	cFF12H
monomer	67.9	24.6	13.8	5.3
dimer	30.6	50.3	67.7	66.9
trimer	1.5	17.0	15.8	22.8
tetramer	0.019	5.7	2.5	4.2
pentamer	0	1.9	0.20	0.59
hexamer	0	0.37	0.0056	0.50
heptamer	0	0.071	0	0.0055
octamer	0	0.056	0	0
nonamer	0	0.027	0	0

In the case of the charged FF peptide (uFF12L and uFF12H), there is a dramatic change in the oligomer size distribution as the concentration increases (here by a factor of about 2.5). The frequency of the monomeric state decreases significantly at the expense of higher order oligomeric states (up to and including nonamers). In particular, there is a significant depletion of monomeric states from the majority population at 68 to 25%. On the other hand, there is very little change in the uncharged FF's oligomer size distribution upon an analogous increase in concentration. Interestingly, most of the uncharged FF peptides remain in dimeric states (67%), and no octamers and nonamers are found. This result seems at first counterintuitive, as one might expect the uncharged case to have higher hydrophobic character and thus display stronger tendencies toward aggregation. However, a strong possibility is that the zwitterionic form displays behavior that is more reminiscent of amphiphiles, where both polar and hydrophobic groups contribute to structuring higher-order aggregates in a manner that is strongly concentration-dependent.

To gain a deeper insight into the actual structures formed in these simulations, we use a clustering technique to identify dominant configurations at each oligomer size. Figure 7 shows the configurations for dimers (top) to nonamers/heptamers (bottom) of charged FF (left, panel a) and uncharged FF (right, panel b) peptides. An immediately obvious difference between the two peptide forms is that substantial side-chain stacking is evident in Figure 7a but is less prominent in Figure 7b. Indeed, the oligomers of the uncharged FF peptides appear more "disordered" in visual terms; in many cases, there is clustering of a few side chains, but several others extend into the solution away from the center of the oligomer. On the other hand, the emergence of ordered stacking arrangements is quite apparent in the zwitterionic case. Most importantly, charged FF peptides form much higher-order oligomers at the same concentration, although the frequencies of these higher-order oligomers are very low (Table 2).

Figure 7 suggests an appealing interpretation of the zwitterionic FF peptides in terms of a hierarchy of association

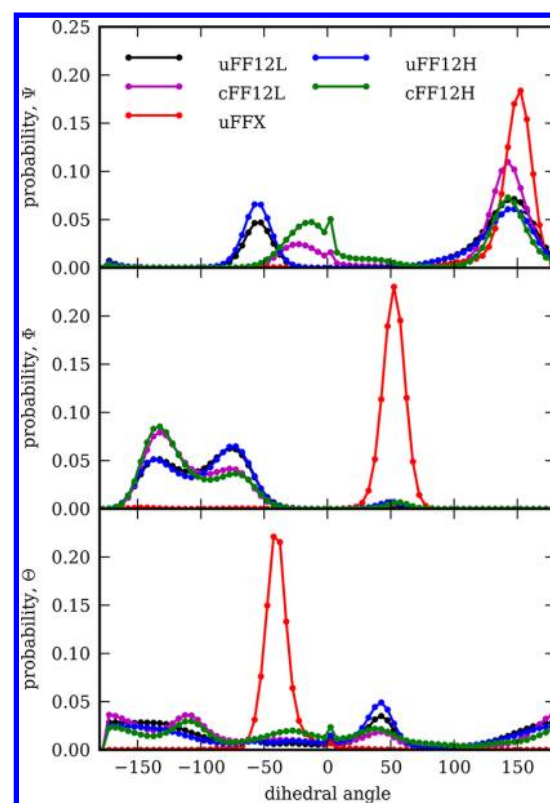


**Figure 6.** Probability distributions of the dihedral angles of FF as defined in Figure 2. uFFX is the reference probability distribution from the crystal structure.

events at different oligomer sizes. In small oligomers, FF peptides tend to reduce their exposure to solvent by stacking of their side chains and exposing their backbones to solvent in a manner consistent with hydrophobic interactions. As additional monomers add to these small-scale aggregates, they form parallel beta-sheet-like "ladder" structures stabilized by hydrogen bonds and salt bridges. A ladder typically contains two or three peptides stitched together along the backbone, and it presents a hydrophobic face with the majority of side-chains on one side of the sheet. Such faces promote a convenient interface for the addition of further monomers or can zip together with other ladders. In this sense, polar interactions appear to "steer" oligomers into structures that prealign and favorably organize hydrophobic groups, while the latter provide an overall driving force for association. The octamer configuration in Figure 7a, for example, shows a combination of three dimer ladders with additional FF peptides. Remarkably, these ladder-like configurations have significant similarities with parts of the nanotube crystal structure *in between* its hydrophilic pores, rather than within a single pore. By comparison, the uncharged peptide shows fewer structural signatures or distinct ladder configurations, although many of the larger oligomers in Figure 7b do appear to contain dimers that are (loosely) held together by polar interactions. In addition, substantial clustering and stacking of hydrophobic side chains seems to drive the organization of these oligomers.

These early oligomers suggest that FF peptides might first assemble into structures that form portions of the packed hydrophobic regions in the nanotube walls, rather than the six-membered rings that define the small pores, as was suggested in an earlier simulation study.<sup>30</sup> Indeed, a picture in which the

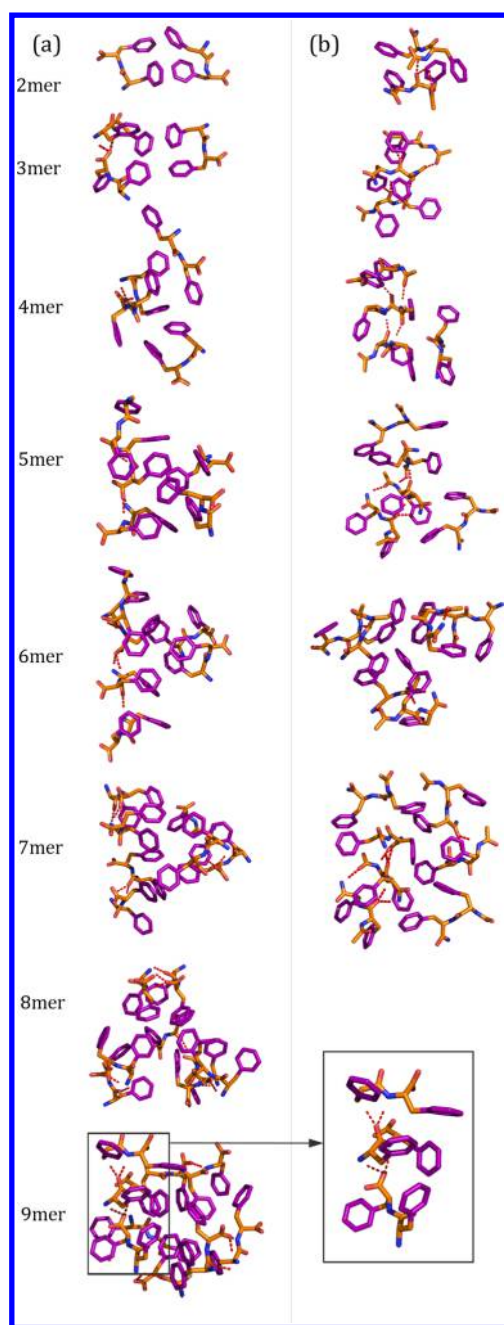


**Figure 7.** Oligomer configurations for dimers to nonamer/heptamers found from clustering the high-concentration MD simulations of 12 (a) charged and (b) uncharged peptides. The aromatic rings of the FF side chains are colored purple to more clearly illustrate their packing. Salt bridges and hydrogen bonds are shown as dotted red lines. The boxed trimer in the bottom right shows an image of a typical “ladder” configuration in which interpeptide polar interactions form a beta-sheet-like structure and align the majority of hydrophobic side chains on one of its sides. The configuration is taken directly from the 9mer structure shown for the zwitterionic peptide.

hydrophobic or aromatic interactions drive the growth of small peptide clusters is generally more consistent with the experimental observation that uncharged peptides retain the ability to form nanotubes. These first structures would then have hydrophilic surfaces and hydrophobic interiors that could later be stitched together by electrostatic interactions at the termini to form the ring motifs.

The contact maps in Figure 3c and d help reveal the relative underlying roles of electrostatics and hydrophobic interactions in zwitterionic FF oligomerization. Comparing the “low” and “high” concentration cases, electrostatic-dominated interactions and contacts show similar behavior; the probabilities of termini–termini, backbone–backbone, and C-termini–backbone interactions are roughly the same. However, the probability of side chain–side chain interactions shows a slight but noticeable change upon increasing the concentration that is suggestive of the role of hydrophobic and aromatic interactions. Namely, one finds that the probability for contacts between pairs of second rings (atoms 14–19) increases and that for contacts between charged ends decreases (atoms 0, 21, and 22). The structure actually becomes more similar to that of the crystal (Figure 3g), in which the second rings have a stronger pair interaction due to their close packing (red circle in Figure 1). Thus, it appears that increases in the local concentration of zwitterionic FF peptides lead to concomitant increases in the numbers of higher-order oligomers, which in turn promote attractions and structuring among the side chains that become closer to those of the crystal structure.

It is interesting to note one important difference between the high-concentration oligomer contact map (Figure 3d) and that of the reference crystal structure (Figure 3g). The latter shows contacts between the termini that are much less frequent and hence may make a smaller contribution to stability as compared to the side chain interactions. This is despite the fact that opposite-charged termini are in close contact in the hexagonal ring structure of the crystal and are able to form strong salt-bridges. As discussed earlier, this suggests a strong role in the crystal for side-chain packing, aromatic stacking, and hydrophobic interactions as compared to the salt-bridges. In contrast in the oligomer simulation, the termini contacts are more frequent than side-chain ones and are in fact the most stable interactions as assessed by the contact probabilities. This comparison shows that electrostatic driving forces can indeed remain significant to the structures found during the early formation pathway of the nanotubes but may become less relevant once larger oligomers adopt the constraints of the crystal structure. Indeed, the small pores throughout the crystal contain water that can to a small extent screen salt-bridge interactions; moreover, that the termini are positioned near these fluid regions permits enhanced conformational fluctuations as compared to the tightly packed side chains. Synthesizing all of these results, we might hypothesize that the attraction between side chains provides a strong driving force for zwitterionic FF peptides to aggregate at high oligomer numbers and in a manner that promotes packing of the aromatic rings, while electrostatic interactions from the termini direct the very small oligomer structures and can act to steer peptides into a more ordered state.

By comparison, Figure 3e and f shows that the contact probabilities for oligomers of the uncharged FF peptides show much weaker preferences for specific interactions. Moreover, an increase in concentration has but a small effect on the overall behavior of the relative contact frequencies. We do see several hydrogen bonds in the clustered structures of uncharged FF oligomers (Figure 7b), although the contact probabilities of backbone–backbone and end–end remain somewhat unpronounced. To a small extent, there are higher probabilities for ring–ring contacts that do emphasize the role for hydrophobic and stacking interactions in uncharged FF self-assembly as well. Unfortunately, however, it is not known at present whether or



not the atomic structure of nanotubes formed from capped FF peptides remains identical to the zwitterionic case. Therefore, we cannot make any definitive conclusions about the similarities of these oligomer structures to experiments at this time.

Returning to the zwitterionic case, a final way to compare oligomer structures with the crystal structure is through an analysis of several key dihedral angles. In addition to the usual  $\Psi$  ( $\text{N}-\text{C}_\alpha-\text{C}-\text{N}$ ) and  $\Phi$  ( $\text{C}-\text{N}-\text{C}_\alpha-\text{C}$ ) backbone torsional angles in the peptide, a third relevant angle  $\Theta$  is the one that defines whether the two side chains are in a *cis* or *trans* orientation. Figure 2 gives an illustration of these three angles. In the crystal structure, these dihedrals adopt unique average values: 157.8, 55.4, and  $-40.2^\circ$  for  $\Psi$ ,  $\Phi$ , and  $\Theta$ , respectively. One of the most interesting observations is that  $\Theta$  differs substantially from what is found for the isolated peptide (dilute solution) and in fact for most of zwitterionic dipeptides, where  $|\Theta| > 135^\circ$ , as typically found in the Cambridge Structural Database.<sup>40</sup> That is, the crystal has a *cis* arrangement of the side chains, while for the individual peptide a *trans* conformation is more favorable. It therefore appears that the peptides must perform an internal *trans*-to-*cis* rearrangement during the nanotube self-assembly process. We partially see this transition already at the stage of dimerization, as discussed above, and certainly for the larger oligomers that display side-chain stacking.

The solution-phase oligomer simulations show that the angle  $\Theta$  is generally very broadly distributed and has high populations near  $\pm 180^\circ$ , the *trans* state, and another smaller population near  $+40^\circ$ , a *cis* conformation but one whose angle differs in sign from that of the crystal (Figure 6). It is interesting to observe that, as the concentration of the oligomers increases, the population in all *cis* states also increases, at the expense of *trans* conformations. This may be further evidence that, at higher concentrations and larger oligomer sizes, the thermodynamically favored structures move closer to the crystal motifs.

There are also interesting signals of structural changes in the backbone torsional angles. We find bimodal distributions of the  $\Psi$  angle. Oddly, in this case, higher oligomer concentrations shift the balance between the two peaks further away from the crystal structure. On the other hand, three peaks are found in the  $\Phi$  distribution, two which overlap in the negative angle regime. Here, the crystal structure only contains the narrow, singly peaked positive angle, but an increase in concentration does shift the oligomer distributions toward increasing magnitudes of this peak. For the zwitterionic version of the peptides, the backbone torsion angles show the formation of  $\beta$ -sheet-like structures ( $100 < \Psi < 180$  and  $-150 < \Phi < -50$ ), whereas the capped peptides form both  $\alpha$ -helix ( $-50 < \Psi < 0$  and  $-150 < \Phi < -50$ ) and  $\beta$ -sheet-like structures. Thus, the general trend is that two of the three angle distributions move closer toward that of the crystal as higher-order oligomers are formed, although they are still far from attaining quantitative agreement and backbone rotations around  $\text{C}_\beta-\text{C}$  ( $\Psi$  angle) and around  $\text{N}-\text{C}_\alpha$  ( $\Phi$  angle) still show a much broader and distinct average direction. The difference may stem from differences in hydrogen bonding: the oligomers have hydrogen bonds between the amino H atom and the backbone oxygen atom,  $-\text{NH}_3^+\cdots\text{O}=\text{C}-$ , that are not seen in the crystal. Overall, these oligomers are still distinct from the perfect crystal structure, which may in fact require much larger cluster sizes than the ones simulated here.

## CONCLUSIONS

FF peptides self-assemble into nanotubes with a unique molecular structure. To better understand this process, here we investigated the association behavior of small FF oligomers using a variety of all-atom simulation techniques. Our results using extensive explicit molecular dynamics simulations suggest several driving forces and structural motifs that dictate early assembly. Zwitterionic FF peptides with charged termini achieve more ordered, clustered, and compact states than those of uncharged FF peptides by means of electrostatic steering. Namely, we find that FF oligomers associate by hydrophobic interactions between side chains but that electrostatic interactions between zwitterionic FF peptides steer their backbones into a more ordered state, forming dimer and trimer peptide “ladders”. These structures, in turn, facilitate hydrophobic-driven association of the side chains in higher order oligomers. This picture is consistent with one where the amphipathic nature of the peptides is central to early assembly. It is in contrast to earlier hypotheses that ring-like peptide hexamers might form due to salt-bridge interactions, similar to what is seen in the FFNT crystal structure. Here, our simulations suggest that instead the motifs corresponding to the dense hydrophobic regions in the nanotube walls might be more relevant to the initial assembly pathway.

For comparison, we also perform simulations of the crystal structure itself, and find that the most prevalent atom–atom contacts are those involving side-chain packing, while polar interactions between peptide termini are comparatively less frequent. This result is arguably consistent with experiments demonstrating that charged termini are not essential for FF’s ability to form nanotubes. We also find that zwitterionic FF oligomers formed from solution become more similar in structure to the crystal at higher concentrations, particularly in a manner in which the side-chains interact. However, we still see outstanding differences in specific structural metrics; most notably, the backbone dihedral angles of FF peptides are broadly distributed in small oligomers, indicating that a highly stable structural motif has yet to be formed. It is quite likely that the minimum oligomer size that forms a stable structural motif similar to the one seen in the crystal structure is greater than the rather small peptide copy number of 12 investigated here.

Given the growing attention to FF peptides as novel materials, these simulations may provide insights for further understanding FF’s self-assembly mechanisms and may ultimately be useful for the design of phenylalanine-based biomolecular nanostructures. It would be particularly interesting to use such approaches not only to study the number of other FF analogues and mutants that have been examined experimentally but also to investigate the self-assembly of single phenylalanine amino acids. Very recently, it has been suggested that phenylalanine itself forms fibrils in brain tissues and might have a possible role in phenylketonuria.<sup>43</sup> Further simulation studies could shed light on the phenylalanine self-assembly mechanism and its relationship to the diphenylalanine family.

## ASSOCIATED CONTENT

### Supporting Information

The methods and results from simulations using the GBSA implicit water model. This material is available free of charge via the Internet at <http://pubs.acs.org>.

## AUTHOR INFORMATION

### Corresponding Author

\*Phone: +1 805 893 4346. E-mail: shell@engineering.ucsb.edu.

### Notes

The authors declare no competing financial interest.

## ACKNOWLEDGMENTS

The authors greatly appreciate the support of the National Science Foundation (Award No. CBET-0845074) and of the Beckman Scholars Program through the Arnold and Mabel Beckman Foundation. The authors also acknowledge stimulating discussions with P. Daugherty.

## ABBREVIATIONS

FF, diphenylalanine; FFNT, diphenylalanine nanotube; MD, molecular dynamics; REMD, replica-exchange molecular dynamics; UREMD, umbrella sampling replica-exchange molecular dynamics; PMF, potential of mean force

## REFERENCES

- Reches, M.; Gazit, E. Casting Metal Nanowires within Discrete Self-Assembled Peptide Nanotubes. *Science* **2003**, *300*, 625–627.
- Sedman, V. L.; Adler-Abramovich, L.; Allen, S.; Gazit, E.; Tendler, S. J. B. Direct Observation of the Release of Phenylalanine from Diphenylalanine Nanotubes. *J. Am. Chem. Soc.* **2006**, *128*, 6903–6908.
- Adler-Abramovich, L.; Reches, M.; Sedman, V. L.; Allen, S.; Tendler, S. J. B.; Gazit, E. Thermal and Chemical Stability of Diphenylalanine Peptide Nanotubes: Implications for Nanotechnological Applications. *Langmuir* **2006**, *22*, 1313–1320.
- Kol, N.; Adler-Abramovich, L.; Barlam, D.; Shneck, R. Z.; Gazit, E.; Rousso, I. Self-Assembled Peptide Nanotubes Are Uniquely Rigid Bioinspired Supramolecular Structures. *Nano Lett.* **2005**, *5*, 1343–1346.
- Yan, X.; Zhu, P.; Li, J. Self-Assembly and Application of Diphenylalanine-Based Nanostructures. *Chem. Soc. Rev.* **2010**, *39*, 1877–1890.
- Rosenman, G.; Beker, P.; Koren, I.; Yevnin, M.; Bank-Srouer, B.; Mishina, E.; Semin, S. Bioinspired Peptide Nanotubes: Deposition Technology, Basic Physics and Nanotechnology Applications. *J. Pept. Sci.* **2011**, *17*, 75–87.
- Hauser, C. A. E.; Zhang, S. Nanotechnology: Peptides as Biological Semiconductors. *Nature* **2010**, *468*, 516–517.
- Amdursky, N.; Molotskii, M.; Aronov, D.; Adler-Abramovich, L.; Gazit, E.; Rosenman, G. Blue Luminescence Based on Quantum Confinement at Peptide Nanotubes. *Nano Lett.* **2009**, *9*, 3111–3115.
- Kholkin, A.; Amdursky, N.; Bdikin, I.; Gazit, E.; Rosenman, G. Strong Piezoelectricity in Bioinspired Peptide Nanotubes. *ACS Nano* **2010**, *4*, 610–614.
- Heredia, A.; Bdikin, I.; Kopyl, S.; Mishina, E.; Semin, S.; Sigov, A.; German, K.; Bystrov, V.; Gracio, J.; Kholkin, A. L. Temperature-Driven Phase Transformation in Self-Assembled Diphenylalanine Peptide Nanotubes. *J. Phys. D: Appl. Phys.* **2010**, *43*, 462001.
- Ryu, J.; Lim, S. Y.; Park, C. B. Photoluminescent Peptide Nanotubes. *Adv. Mater.* **2009**, *21*, 1577–1581.
- Han, T. H.; Oh, J. K.; Park, J. S.; Kwon, S.-H.; Kim, S.-W.; Kim, S. O. Highly Entangled Hollow TiO<sub>2</sub> Nanoribbons Templating Diphenylalanine Assembly. *J. Mater. Chem.* **2009**, *19*, 3512.
- Mahler, A.; Reches, M.; Rechter, M.; Cohen, S.; Gazit, E. Rigid, Self-Assembled Hydrogel Composed of a Modified Aromatic Dipeptide. *Adv. Mater.* **2006**, *18*, 1365–1370.
- Yemini, M.; Reches, M.; Rishpon, J.; Gazit, E. Novel Electrochemical Biosensing Platform Using Self-Assembled Peptide Nanotubes. *Nano Lett.* **2004**, *5*, 183–186.
- Yemini, M.; Reches, M.; Gazit, E.; Rishpon, J. Peptide Nanotube-Modified Electrodes for Enzyme–Biosensor Applications. *Anal. Chem.* **2005**, *77*, 5155–5159.
- Cipriano, T.; Takahashi, P.; De Lima, D.; Oliveira, V.; Souza, J.; Martinho, H.; Alves, W. Spatial Organization of Peptide Nanotubes for Electrochemical Devices. *J. Mater. Sci.* **2010**, *45*, 5101–5108.
- Sopher, N. B.; Abrams, Z. R.; Reches, M.; Gazit, E.; Hanein, Y. Integrating Peptide Nanotubes in Micro-Fabrication Processes. *J. Micromech. Microeng.* **2007**, *17*, 2360–2365.
- Adler-Abramovich, L.; Aronov, D.; Beker, P.; Yevnin, M.; Stempler, S.; Buzhansky, L.; Rosenman, G.; Gazit, E. Self-assembled Arrays of Peptide Nanotubes by Vapour Deposition. *Nat. Nanotechnol.* **2009**, *4*, 849–854.
- Beker, P.; Koren, I.; Amdursky, N.; Gazit, E.; Rosenman, G. Bioinspired Peptide Nanotubes as Supercapacitor Electrodes. *J. Mater. Sci.* **2010**, *45*, 6374–6378.
- Gorbitz, C. H. The Structure of Nanotubes Formed by Diphenylalanine, the Core Recognition Motif of Alzheimer's beta-amyloid Polypeptide. *Chem. Commun.* **2006**, 2332.
- Görbitz, C. H. Nanotube Formation by Hydrophobic Dipeptides. *Chem.—Eur. J.* **2001**, *7*, 5153–5159.
- Reches, M.; Gazit, E. Self-Assembly of Peptide Nanotubes and Amyloid-Like Structures by Charged-Termini-Capped Diphenylalanine Peptide Analogues. *Isr. J. Chem.* **2005**, *45*, 363–371.
- Mishra, A.; Chauhan, V. S. Probing the Role of Aromaticity in the Design of Dipeptide Based Nanostructures. *Nanoscale* **2011**, *3*, 945.
- Reches, M.; Gazit, E. Formation of Closed-Cage Nanostructures by Self-Assembly of Aromatic Dipeptides. *Nano Lett.* **2004**, *4*, 581–585.
- Govindaraju, T.; Pandeeswar, M.; Jayaramulu, K.; Jaipuria, G.; Atreya, H. S. Spontaneous Self-Assembly of Designed Cyclic Dipeptide (Phg-Phg) into Two-Dimensional Nano- and Mesosheets. *Supramol. Chem.* **2011**, *23*, 487–492.
- Han, T. H.; Oh, J. K.; Lee, G.-J.; Pyun, S.-I.; Kim, S. O. Hierarchical Assembly of Diphenylalanine into Dendritic Nano-architectures. *Colloids Surf., B* **2010**, *79*, 440–445.
- Tsai, C.-J.; Zheng, J.; Nussinov, R. Designing a Nanotube Using Naturally Occurring Protein Building Blocks. *PLoS Comput. Biol.* **2006**, *2*, e42.
- Flöck, D.; Rossetti, G.; Daidone, I.; Amadei, A.; Nola, A. D. Aggregation of Small Peptides Studied by Molecular Dynamics Simulations. *Proteins* **2006**, *65*, 914–921.
- Song, Y.; Challa, S. R.; Medforth, C. J.; Qiu, Y.; Watt, R. K.; Pena, D.; Miller, J. E.; van Swol, F.; Shelnutt, J. A. Synthesis of Peptide-Nanotube Platinum-Nanoparticle Composites. *Chem. Commun.* **2004**, 1044.
- Tamamis, P.; Adler-Abramovich, L.; Reches, M.; Marshall, K.; Sikorski, P.; Serpell, L.; Gazit, E.; Archontis, G. Self-Assembly of Phenylalanine Oligopeptides: Insights from Experiments and Simulations. *Biophys. J.* **2009**, *96*, 5020–5029.
- Guo, C.; Luo, Y.; Zhou, R.; Wei, G. Probing the Self-Assembly Mechanism of Diphenylalanine-Based Peptide Nanovesicles and Nanotubes. *ACS Nano* **2012**, *6*, 3907–3918.
- Pearlman, D. A.; Case, D. A.; Caldwell, J. W.; Ross, W. S.; Cheatham, T. E.; DeBolt, S.; Ferguson, D.; Seibel, G.; Kollman, P. AMBER, a Package of Computer Programs for Applying Molecular Mechanics, Normal Mode Analysis, Molecular Dynamics and Free Energy Calculations to Simulate the Structural and Energetic Properties of Molecules. *Comput. Phys. Commun.* **1995**, *91*, 1–41.
- Case, D. A.; Cheatham, T. E., 3rd; Darden, T.; Gohlke, H.; Luo, R.; Merz, K. M., Jr.; Onufriev, A.; Simmerling, C.; Wang, B.; Woods, R. J. The Amber Biomolecular Simulation Programs. *J. Comput. Chem.* **2005**, *26*, 1668–1688.
- Onufriev, A.; Bashford, D.; Case, D. A. Modification of the Generalized Born Model Suitable for Macromolecules. *J. Phys. Chem. B* **2000**, *104*, 3712–3720.
- Baker, N. A. Improving Implicit Solvent Simulations: a Poisson-Centric View. *Curr. Opin. Struct. Biol.* **2005**, *15*, 137–143.



- (36) Mobley, D. L.; Dill, K. A.; Chodera, J. D. Treating Entropy and Conformational Changes in Implicit Solvent Simulations of Small Molecules. *J. Phys. Chem. B* **2008**, *112*, 938–946.
- (37) Mobley, D. L.; Bayly, C. L.; Cooper, M. D.; Shirts, M. R.; Dill, K. A. Small Molecule Hydration Free Energies in Explicit Solvent: An Extensive Test of Fixed-Charge Atomistic Simulations. *J. Chem. Theory Comput.* **2009**, *5*, 350–358.
- (38) Strodel, B.; Wales, D. J. Implicit Solvent Models and the Energy Landscape for Aggregation of the Amyloidogenic KFFE Peptide. *J. Chem. Theory Comput.* **2008**, *4*, 657–672.
- (39) van Gunsteren, W. F.; Weiner, P. K.; Wilkinson, A. J. *Computer Simulation of Biomolecular Systems: Theoretical and Experimental Applications*; Vol. 3; ESCOM Science Publishers: Leiden, The Netherlands, 1997.
- (40) Görbitz, C. H. Nanotube Formation by Hydrophobic Dipeptides. *Chem.—Eur. J.* **2001**, *7*, 5153–5159.
- (41) Dill, K. A.; Ozkan, S. B.; Shell, M. S.; Weikl, T. R. The Protein Folding Problem. *Annu. Rev. Biophys.* **2008**, *37*, 289–316.
- (42) Lloyd, S. Least Squares Quantization in PCM. *IEEE Trans. Inf. Theory* **1982**, *28*, 129–137.
- (43) Adler-Abramovich, L.; Vaks, L.; Carny, O.; Trudler, D.; Magno, A.; Cafisch, A.; Frenkel, D.; Gazit, E. Phenylalanine Assembly into Toxic Fibrils Suggests Amyloid Etiology in Phenylketonuria. *Nat. Chem. Biol.* **2012**, *8*, 701–706.